SUPPORTING INFORMATION

Evaluation of the daytime tropospheric loss of 2-methylbutanal

María Asensio[1,2], María Antiñolo[1,2,†], Sergio Blázquez[2], José Albaladejo[1,2], Elena Jiménez[1,2,*]

[1]Instituto de Investigación en Combustión y Contaminación Atmosférica, Universidad de Castilla-La Mancha, Camino de Moledores s/n, Ciudad Real, 13071, Spain
[2]Departamento de Química Física, Universidad de Castilla-La Mancha, Avda. Camilo José Cela 1B, Ciudad Real, 13071, Spain

Correspondence to: Elena Jiménez (elena.jimenez@uclm.es)

[†] Currently at *Escuela* de *Ingeniería Industrial* y *Aeroespacial*. Universidad de Castilla-La Mancha. Avenida Carlos III s/n. Real Fábrica de Armas. 45071 Toledo (Spain).

1. Photochemical experiments of 2-methylbutanal

Gas-phase UV spectroscopy (220-360 nm)

To obtain reliable values of the UV absorption cross section (σ_λ in cm^2 $molecule^{-1}$) several UV spectra were recorded on a gas cell (l = 107.15 cm) using different concentrations of 2MB, as explained in Sect. 2.1.1 of the main text. According to the Beer-Lambert law:

$$A_\lambda = \sigma_\lambda \, l \, [2MB] \qquad \text{(ES1)}$$

the UV absorption cross section at a wavelength λ was obtained from the slope of the measured absorbance (A_λ) *versus* [2MB] plots. In **Fig. S1** some of these plots at several wavelengths are depicted, including the absorption maximum at 296 nm. The obtained UV absorption cross sections are listed in **Table S1** as a function of wavelength.

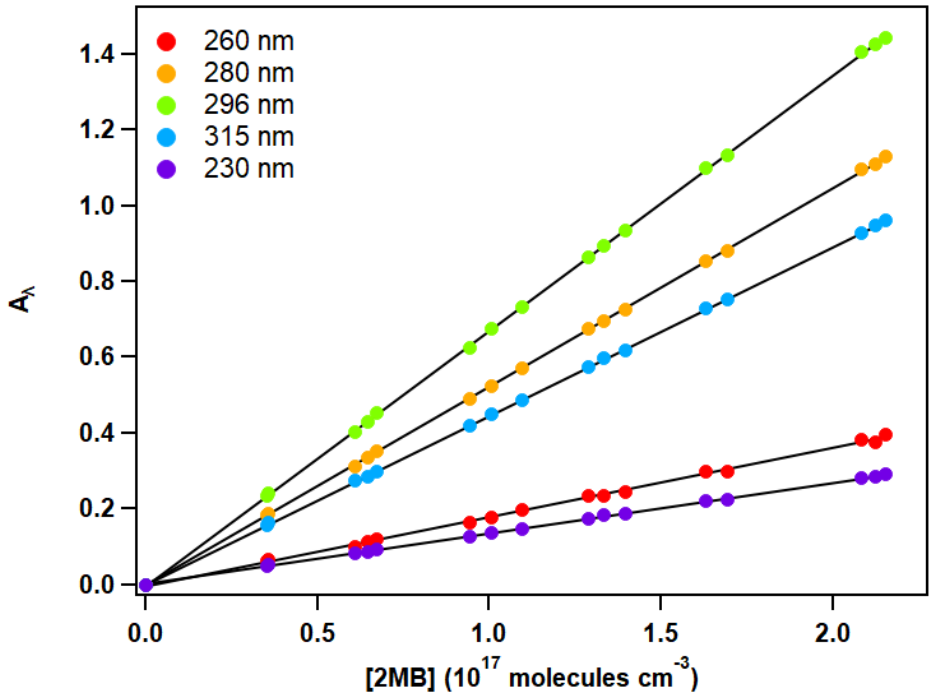

Figure S1: Examples of the Beer-Lambert law plots for 2MB at room temperature.

Table S1. UV absorption cross sections of 2MB (in base *e*) in the range of 220–360 nm at 1-nm intervals. Uncertainties are ±2σ statistical.

λ (nm)	σ_λ (10^{-20} cm^2 molecule^{-1})	λ (nm)	σ_λ (10^{-20} cm^2 molecule^{-1})	λ (nm)	σ_λ (10^{-20} cm^2 molecule^{-1})
220	0.11 ± 0.11	267	2.68 ± 0.07	314	4.32 ± 0.06
221	0.11 ± 0.10	268	2.84 ± 0.07	315	4.17 ± 0.07
222	0.10 ± 0.10	269	3.00 ± 0.08	316	3.97 ± 0.08
223	0.10 ± 0.11	270	3.18 ± 0.09	317	3.72 ± 0.08
224	0.10 ± 0.10	271	3.35 ± 0.09	318	3.45 ± 0.07
225	0.09 ± 0.08	272	3.53 ± 0.06	319	3.18 ± 0.08
226	0.10 ± 0.09	273	3.69 ± 0.07	320	2.97 ± 0.08
227	0.10 ± 0.08	274	3.85 ± 0.07	321	2.79 ± 0.06
228	0.09 ± 0.06	275	4.01 ± 0.09	322	2.61 ± 0.08
229	0.10 ± 0.06	276	4.18 ± 0.08	323	2.44 ± 0.09
230	0.10 ± 0.07	277	4.36 ± 0.08	324	2.28 ± 0.09
231	0.11 ± 0.06	278	4.54 ± 0.07	325	2.13 ± 0.09
232	0.12 ± 0.07	279	4.71 ± 0.07	326	1.97 ± 0.10
233	0.13 ± 0.06	280	4.87 ± 0.07	327	1.82 ± 0.09
234	0.14 ± 0.05	281	5.01 ± 0.08	328	1.65 ± 0.09
235	0.15 ± 0.05	282	5.13 ± 0.08	329	1.46 ± 0.06
236	0.16 ± 0.05	283	5.27 ± 0.07	330	1.27 ± 0.06
237	0.18 ± 0.05	284	5.40 ± 0.08	331	1.09 ± 0.06
238	0.20 ± 0.04	285	5.53 ± 0.08	332	0.94 ± 0.06
239	0.22 ± 0.05	286	5.66 ± 0.09	333	0.82 ± 0.06
240	0.25 ± 0.05	287	5.77 ± 0.10	334	0.72 ± 0.05
241	0.28 ± 0.05	288	5.88 ± 0.08	335	0.63 ± 0.05
242	0.31 ± 0.05	289	5.97 ± 0.10	336	0.54 ± 0.07
243	0.34 ± 0.05	290	6.03 ± 0.09	337	0.47 ± 0.07
244	0.38 ± 0.04	291	6.09 ± 0.07	338	0.41 ± 0.08
245	0.43 ± 0.04	292	6.12 ± 0.08	339	0.35 ± 0.08
246	0.47 ± 0.06	293	6.17 ± 0.07	340	0.30 ± 0.07
247	0.51 ± 0.07	294	6.22 ± 0.09	341	0.25 ± 0.05
248	0.57 ± 0.07	295	6.25 ± 0.07	342	0.20 ± 0.05
249	0.63 ± 0.07	296	6.25 ± 0.08	343	0.15 ± 0.06
250	0.70 ± 0.07	297	6.24 ± 0.07	344	0.11 ± 0.06
251	0.77 ± 0.08	298	6.19 ± 0.08	345	0.08 ± 0.05
252	0.85 ± 0.07	299	6.16 ± 0.05	346	0.06 ± 0.06
253	0.92 ± 0.08	300	6.11 ± 0.07	347	0.05 ± 0.05
254	1.01 ± 0.09	301	6.05 ± 0.07	348	0.05 ± 0.04
255	1.11 ± 0.07	302	5.99 ± 0.09	349	0.04 ± 0.03
256	1.20 ± 0.08	303	5.93 ± 0.09	350	0.04 ± 0.04
257	1.31 ± 0.09	304	5.85 ± 0.08	351	0.04 ± 0.05
258	1.42 ± 0.08	305	5.75 ± 0.08	352	0.04 ± 0.09
259	1.54 ± 0.08	306	5.60 ± 0.09	353	0.03 ± 0.06
260	1.66 ± 0.09	307	5.42 ± 0.07	354	0.03 ± 0.07
261	1.79 ± 0.09	308	5.23 ± 0.08	355	0.03 ± 0.09
262	1.93 ± 0.08	309	5.07 ± 0.09	356	0.04 ± 0.09
263	2.08 ± 0.07	310	4.92 ± 0.08	357	0.03 ± 0.08
264	2.22 ± 0.07	311	4.78 ± 0.08	358	0.03 ± 0.08
265	2.37 ± 0.08	312	4.63 ± 0.07	359	0.03 ± 0.07
266	2.53 ± 0.07	313	4.47 ± 0.07	360	0.03 ± 0.08

Irradiation with a solar simulator (λ≥290 nm)

In **Fig. S2**, the irradiance (I_λ) spectrum of the ABA class solar simulator used in this work is compared with the solar reference spectrum AM 1.5G (grey spectrum), corrected with the intensity measured in this work.

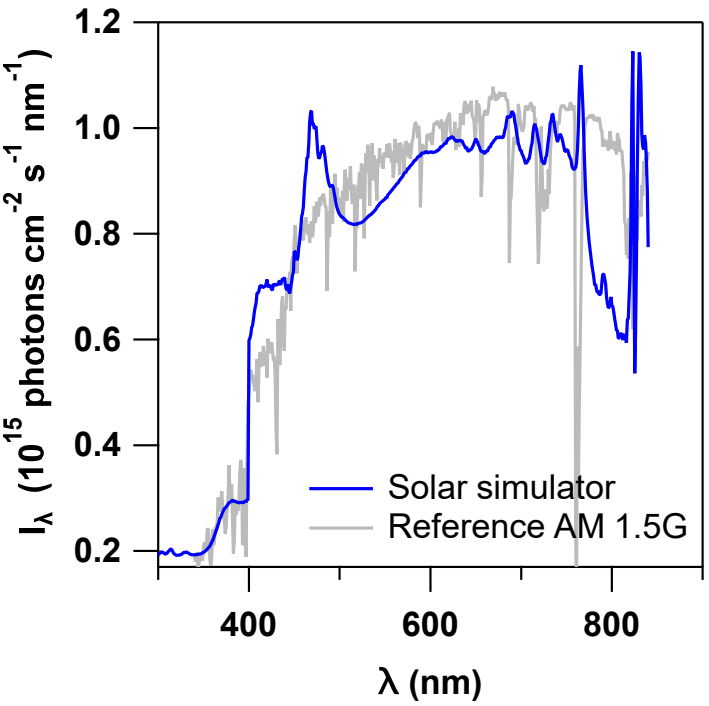

Figure S2: Irradiance spectrum of the ABA class solar simulator used in this work compared with the solar reference spectrum AM 1.5G, corrected with the intensity measured in this work.

2. Absolute kinetic analysis.

The pulsed laser photolysis-laser induced fluorescence (PLP-LIF) technique was used to carry out the OH-kinetic experiments. The experimental set-up and technique have been described in previous publications (Martínez et al., 1999; Albaladejo et al., 2002; Jiménez et al., 2005; Antiñolo et al., 2011; Blázquez et al., 2017). Therefore, only a brief description is given below.

The OH-precursor (H_2O_2 or HNO_3), 2-methylbutanal from a storage bulb, and He as buffer gas were introduced in the 200-mL jacketed Pyrex reactor by means of mass flow controllers. The temperature in the cell was controlled by flowing a heated/cooled liquid (water for T>278 K or a mixture of ethanol/water to achieve temperatures between 268 and 263 K) through the external jacket of the reactor. To evaluate the potential pressure dependence of the rate coefficient of the 2MB+OH reaction, total pressure inside the reactor (P_T) was varied between 50 and 300 Torr over the entire temperature range, and up to 600 torr at room temperature (298 K) and the extreme temperatures (263 and 353 K).

Under *pseudo*-first order conditions ($[2MB]_0$, $[OH\text{-precursor}]_0 >> [OH]_0$), the LIF intensity at a reaction time t ($I_{LIF,t}$) from the OH radicals, produced by 248-nm photolysis of the precursor, was detected as a function of the reaction time t. The temporal profiles of $I_{LIF,t}$ are well-described by a single exponential expression:

$$I_{LIF,t} = I_{LIF,0}\, exp(-k't) \qquad \text{(ES2)}$$

where $I_{LIF,0}$ is the LIF intensity at $t = 0$ and k' is the *pseudo*-first order rate coefficient k' which encompasses all OH-loss processes: reaction with 2MB and the OH-precursor and diffusion out of the detection zone and/or rection with impurities, if present.

$$\text{OH} + \text{2MB} \rightarrow \text{Products} \qquad \text{(RS1)}$$

$$\text{OH} + \text{OH-Precursor} \rightarrow \text{Products} \qquad \text{(RS2)}$$

$$\text{OH} \rightarrow \text{Diffusion and/or reaction with impurities} \qquad \text{(RS3)}$$

In **Fig. S3**, some examples of the decay of the $I_{LIF,t}$ are presented. The analysis of these decays yields k' and k'_0 (k' in absence of 2MB) which is related with the second-order rate coefficient $k_{OH}(T)$ at a given temperature.

$$k' = k_{OH}(T)[2MB]_0 + k'_0 \qquad \text{(ES3)}$$

From the slope of k' (or $k'-k'_0$) *versus* $[2MB]_0$ plots, $k_{OH}(T)$ was determined at every temperature and pressure condition. As an example, **Fig. S4** shows an example of k'-k'_0 *vs* $[2MB]_0$ plot at 263 and 353 K. The concentration of 2MB in the reactor was calculated as follows:

$$[2MB]_0 = 3.24 \times 10^{16} \frac{F_{2MB}}{F_T} f P_T \frac{298\ K}{T(K)} \text{ (molecules cm}^{-3}\text{)} \qquad \text{(ES4)}$$

where

F_{2MB} (in sccm, standard cubic centimeter per minute) is the calibrated mass flow of diluted 2MB from the 10 L storage bulb.

F_T (in sccm) is the total calibrated mass flow (sum of F_{2MB} and the He flow rate through the OH-precursor solution ($F_{He\text{-}Precursor}$) and the additional He flow (F_{He}) needed to obtain the desire [2MB]).

f is the dilution factor of 2MB defined as the $P_{2MB}/(P_{He}+P_{2MB})$ ratio. The total pressure in the storage bulb, $P_{He}+P_{2MB}$, was always close to 750 Torr.

The experimental conditions used in the absolute kinetic experiments of the OH+2MB reaction are listed in **Table S2**. $[2MB]_0$ was varied between 4.1×10^{13} and 5.45×10^{14} molecules cm^{-3}. The f factor of the mixture bulb was checked by UV measurements, considering the obtained UV spectrum of 2MB in this work. The relative error between f measured by pressures and by UV were below 6.7 %. The OH-precursor concentration in the reaction cell was measured at room temperature by gas-phase UV absorption

spectroscopy between 200 and 230 nm, taking into account the reported absorption cross section of H_2O_2 and HNO_3 (Sanders et al., 2011). The experimental HNO_3 range was (0.36 – 10.3) × 10^{15} molecules cm^{-3}, and the H_2O_2 range was (1.6 – 6.2) × 10^{13} molecules cm^{-3}. From these concentrations and considering a quantum yield of OH of 1 for HNO_3 and 2 for H_2O_2, the OH initial concentration was calculated to range from 8.3 × 10^{10} radical cm^{-3} to 5.9 × 10^{12} radical cm^{-3}.

Table S2. Experimental conditions of the kinetic experiments of the OH+2MB reactions and the range of measured *pseudo*-first order rate coefficient.

T **(K)**	$\mathbf{P_T}$ **(Torr)**	$\mathbf{[OH\text{-}Precursor]_0}$ **(10^{13} molecules cm^{-3})**	***f*** **(10^{-4})**	$\mathbf{[2MB]_0}$ **(10^{14} molecules cm^{-3})**	***k'*** **(10^3 s^{-1})**
263	50	439[a]	50.3	0.58 – 5.45	0.3 – 17.0
	300	439[a]	7.96	0.55 – 5.17	1.0 – 16.9
	600	439[a]	3.90	0.54 – 5.07	0.5 – 17.3
268	50	439[a]	50.3	0.57 – 5.35	0.3 – 17.1
	300	439[a]	7.93	0.54 – 4.55	0.7 – 15.2
278	50	6.2[b]	50.8	0.55 – 5.20	0.4 – 14.2
	300	1033[a]	7.96	0.52 – 4.88	0.4 – 14.9
	300	439[a]	7.93	0.52 – 4.87	0.7 – 14.2
288	50	6.0[b]	50.8	0.53 – 5.02	0.2 – 14.0
	300	6.0[b]	7.96	0.50 – 4.73	0.2 – 12.6
	300	6.0[b]	7.96	0.50 – 4.73	0.2 – 15.0
298	50	1.9[b]	50.2	0.52 – 3.44	0.5 – 10.2
	50	1.9[b]	50.2	0.52 – 4.89	0.5 – 13.9
	300	5.8[b]	7.98	0.49 – 4.60	0.5 – 12.5
	600	5.8[b]	4.22	0.51 – 4.85	0.2 – 12.8
309	50	1.8[b]	50.8	0.51 – 4.77	0.5 – 13.7
	300	5.6[b]	7.95	0.47 – 4.40	0.4 – 12.5
323	50	1.8[b]	50.8	0.48 – 4.57	0.4 – 12.1
	300	5.3[b]	7.95	0.45 – 4.21	0.3 – 10.5
338	50	1.7[b]	50.8	0.46 – 4.36	0.3 – 10.6
	300	5.1[b]	7.95	0.43 – 4.02	0.4 – 9.4
353	50	1.6[b]	50.8	0.44 – 3.35	0.3 – 7.9
	300	4.9[b]	7.96	0.41 – 3.86	0.3 – 9.5
	600	36.2[a]	3.97	0.41 – 3.85	0.6 – 9.2

OH radical precursor: [a] HNO_3 and [b] H_2O_2.

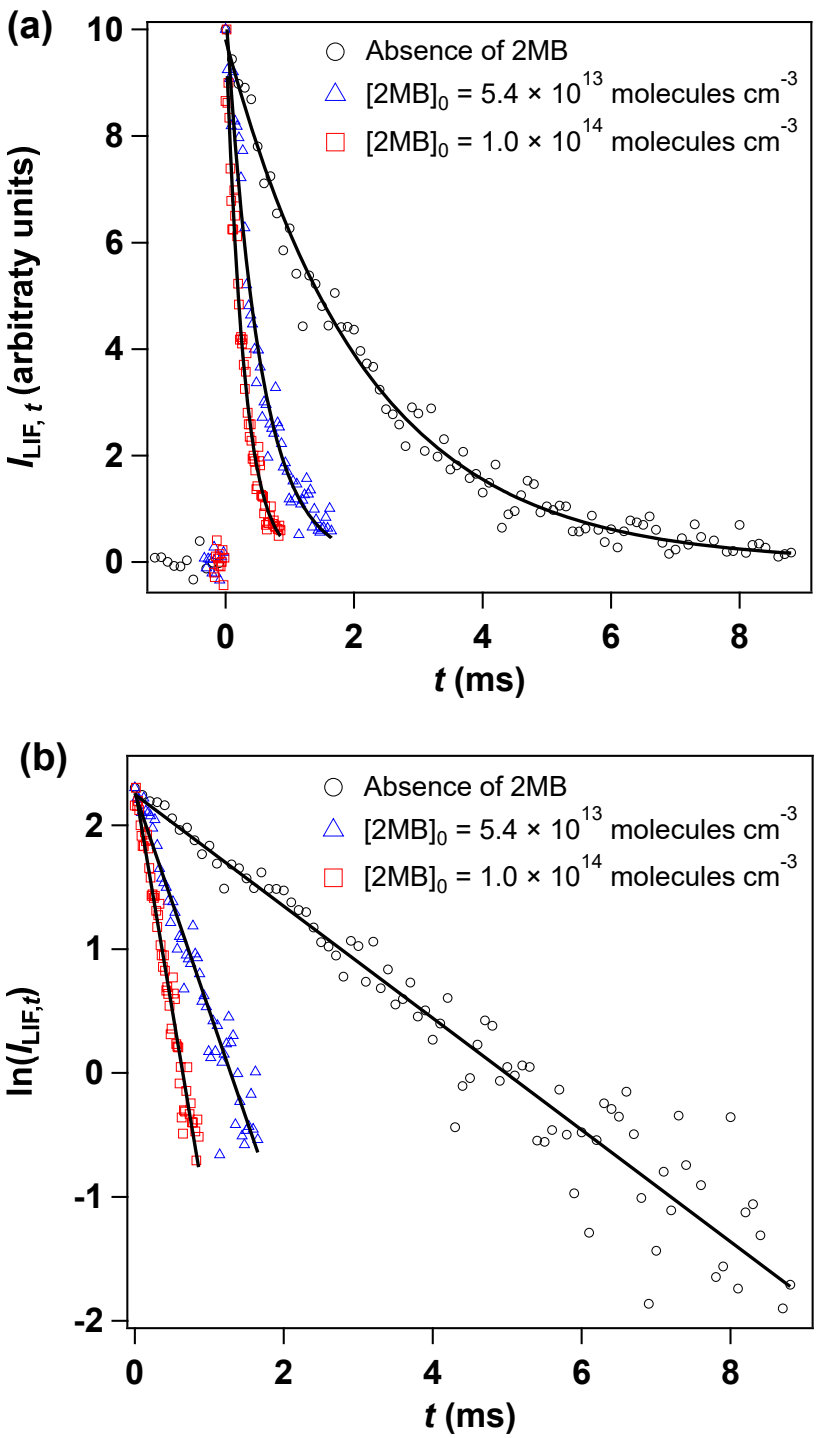

Figure S3: Examples of the LIF temporal profiles in exponential form (a) and linearized form (b) recorded in the absence and presence of 2MB at 263 K and 600 Torr.

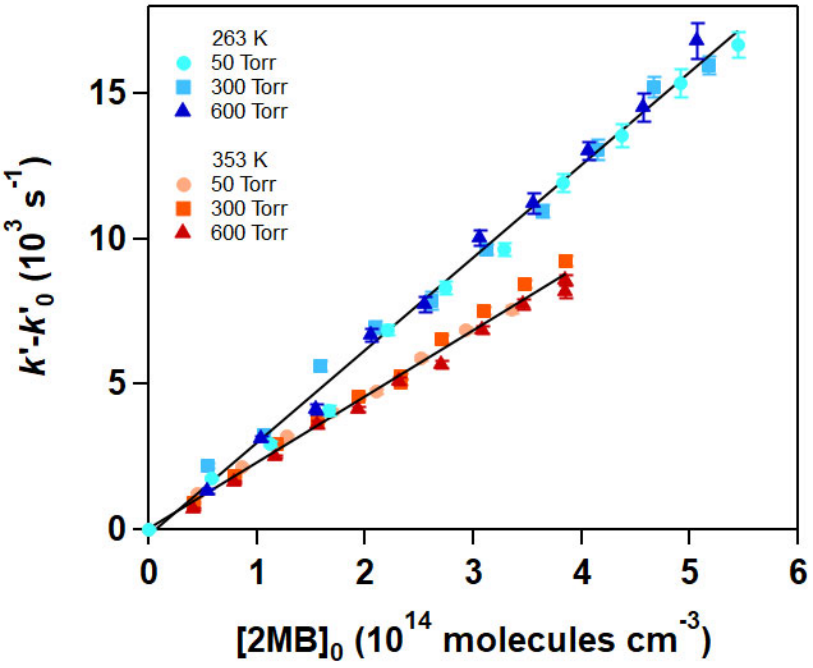

Figure S4: Plots of Eq. (ES3) for the OH+2MB reaction at 263 and 353 K at different total pressures in the reactor.

3. Relative kinetics and product studies.

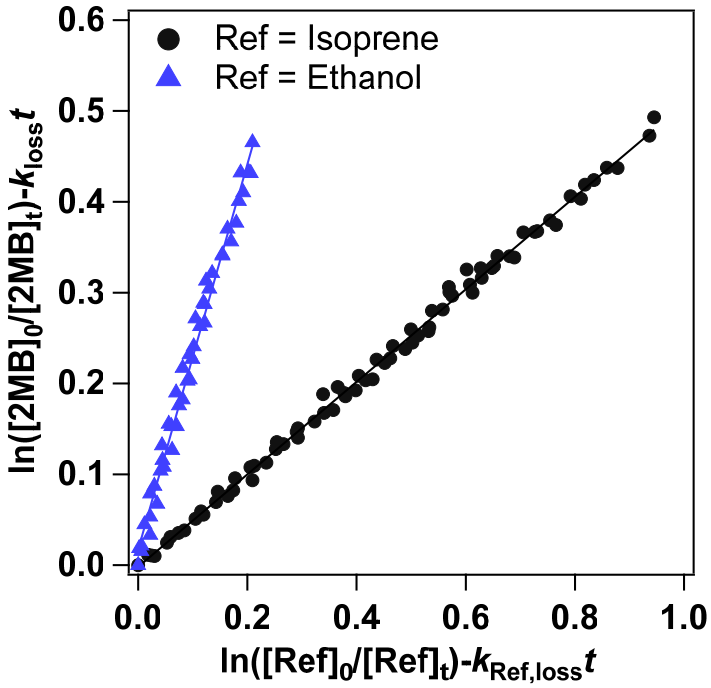

Figure S5: Plots of Eq. (2) for the Cl+2MB reaction using ethanol and isoprene as reference compounds.

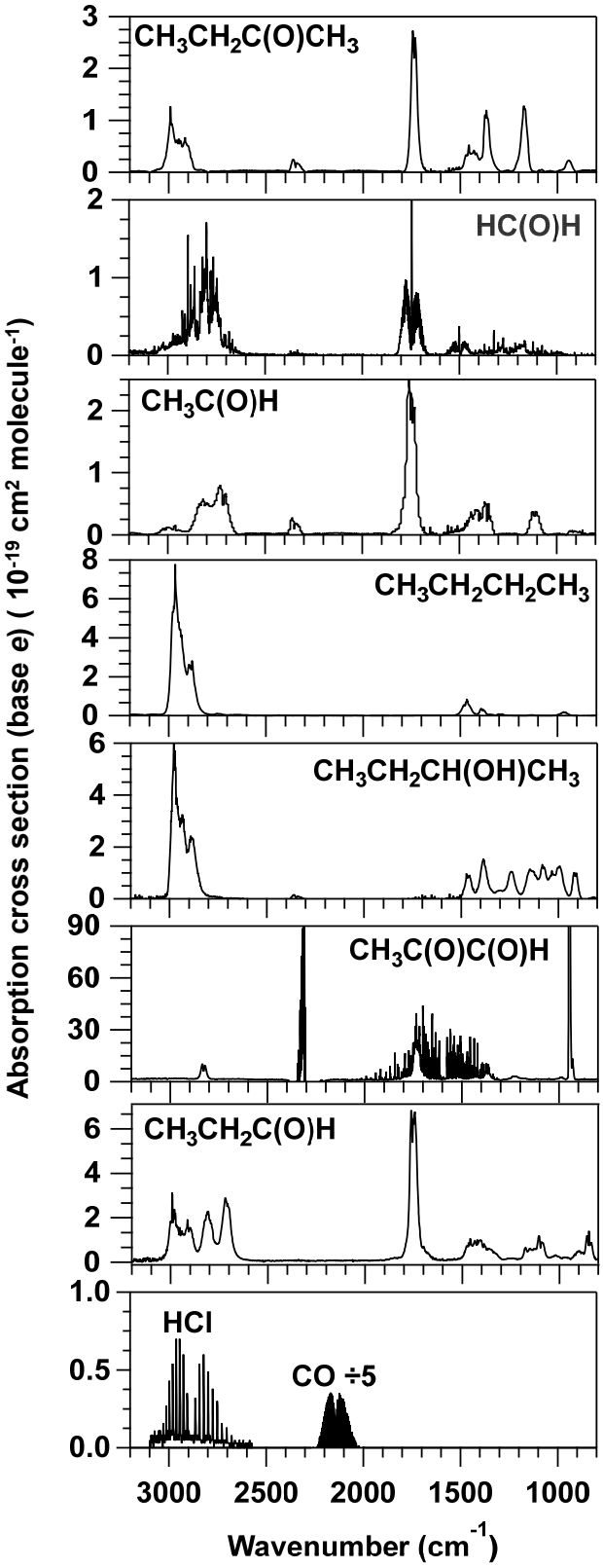

Figure S6: Reference FTIR spectra used in this work. Butanone, formaldehyde, acetaldehyde, propanal, and 2-butanol spectra were recorded in our lab. Butane spectrum was taken from the NIST FTIR database (Linstrom and Mallard, 2018), and methylglyoxal spectrum was taken from the EUROCHAMP database (Ródenas, 2017). CO_2 and H_2O are present as impurities in some of these spectra and were not considered.

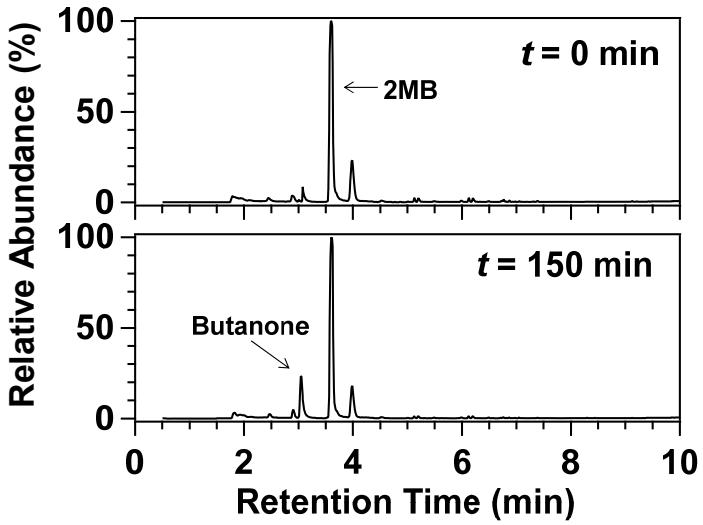

Figure S7: Chromatograms obtained before irradiation (top panel) and after 150 min of photolysis (bottom panel). The most intense peak corresponds to 2MB. Only butanone was detected as a product (retention time, RT = 3.04 min). The small peaks in the chromatogram were due to the degradation of the SPME fibre and the chromatographic column.

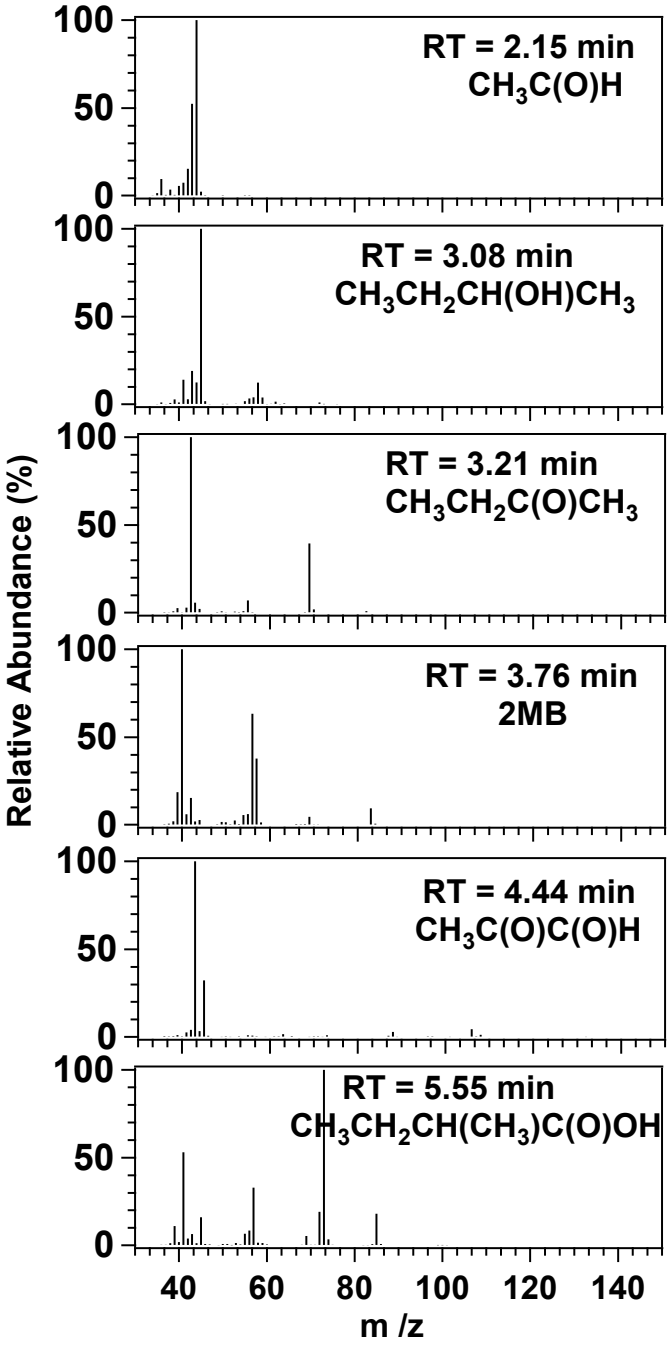

Figure S8: Mass spectra detected for the peaks of the chromatogram shown in Fig. 6 of the paper.

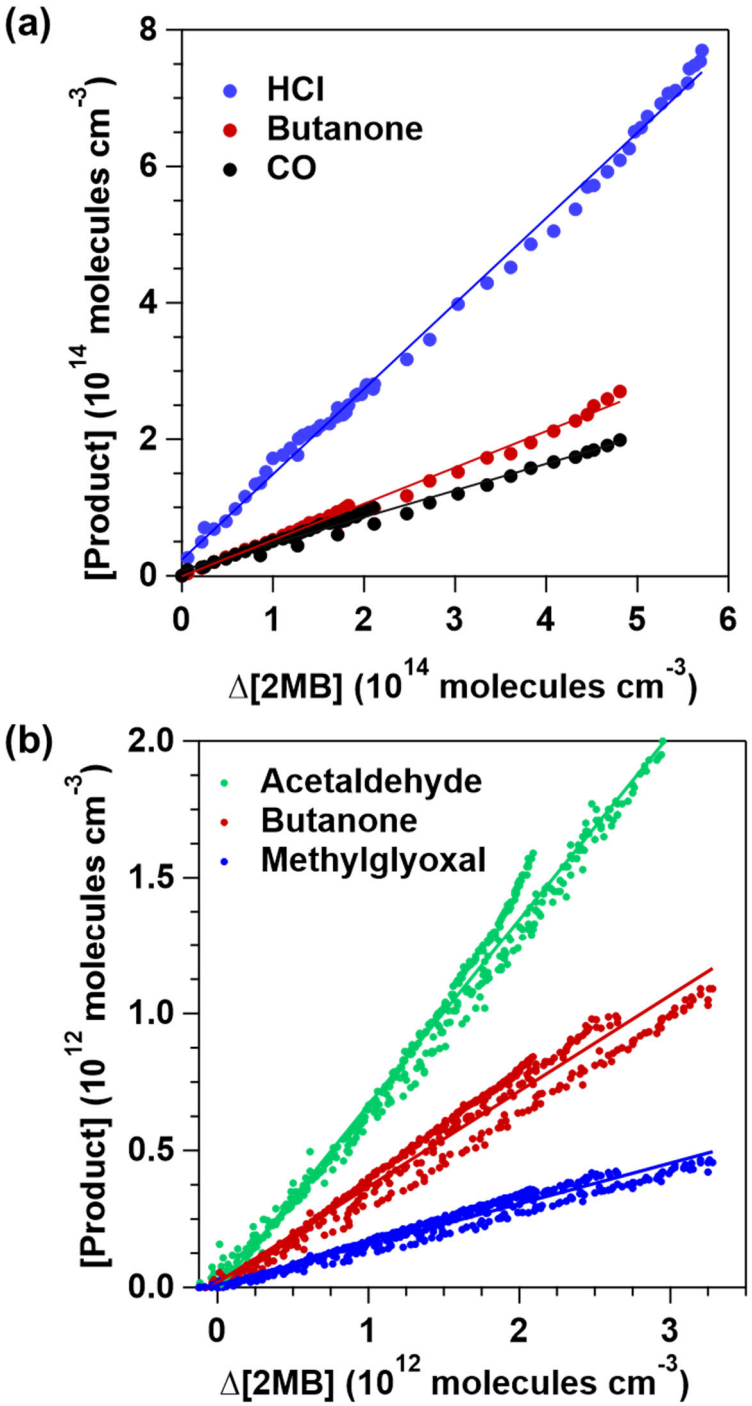

Figure S9: Plots to obtain the product yields in the 2MB + Cl reaction determined by a) FTIR spectroscopy, and b) PTR-ToF-MS. Product concentrations were corrected to account for their Cl-reaction loss as explained by Ceacero-Vega et al. (2012).

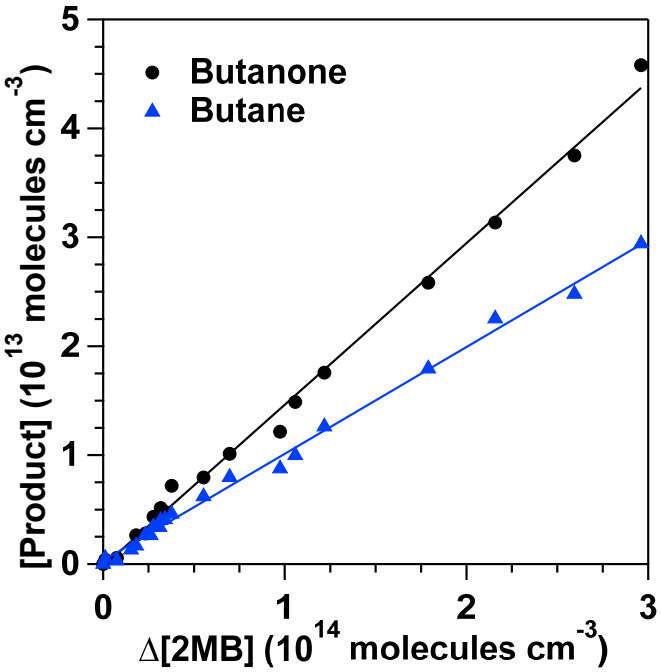

Figure S10. Plots to obtain the product yields in the 2MB photolysis determined by FTIR spectroscopy.

4. Formation of Secondary Organic Aerosols (SOAs) in the Cl + 2MB reaction

For the detection and quantification of the formation of SOAs in the Cl-reaction of 2MB, both the 16-L cell and the 264-L reactor were connected and simultaneously used as described previously (Antiñolo et al., 2020). The concentration of gaseous 2MB was monitored every 2 min by the FTIR spectrometer described in Sect. 2.1.2, whereas the formed SOAs were monitored by a Fast Mobility Particle Sizer (FMPS) spectrometer (TSI 3091). The FMPS spectrometer measures the particle size distribution in the system between 5.6 and 560 nm and every 1 s (although data were averaged for 1 min in this work). A 2MB/Cl_2/air mixture was introduced at (760 ± 5) Torr and (299 ± 2) K in the reactors with concentrations of 2MB and Cl_2 in the (5.5 – 13) × 10^{14} molecules cm^{-3} and (4.8 – 10) × 10^{14} molecules cm^{-3} ranges, respectively. The SOA formation and the loss of 2MB loss was continuously monitored during about 1 hour. During the first 15 min, the gas mixture was kept in the dark to check for SOA formation by dark reactions; then, the lights surrounding the 264-L reactor were turned on for 30-40 min to measure the SOA formed in reaction (R3); finally, the lights were switched off to evaluate the loss of the SOA formed due to the walls or other dark processes during 15 min. The SOA formation yield, Y_{SOA}, can be defined as the ratio between the aerosol mass formed, M_{SOA}, considering a 1.4 μg m^{-3} density for the SOA (Hallquist et al., 2009), and the 2MB lost in reaction (R3), Δ[2MB], (Equation (ES5)).

$$Y_{SOA} = \frac{M_{SOA}}{\Delta[2MB]}, \qquad \text{(ES5)}$$

Both parameters, M_{SOA} and Δ[2MB] were corrected by accounting for their loss as described previously (Antiñolo et al., 2019), and Y_{SOA} was determined from M_{SOA} *versus* Δ[2MB] under different $[2MB]_0$ (see some examples in **Fig. S11**).

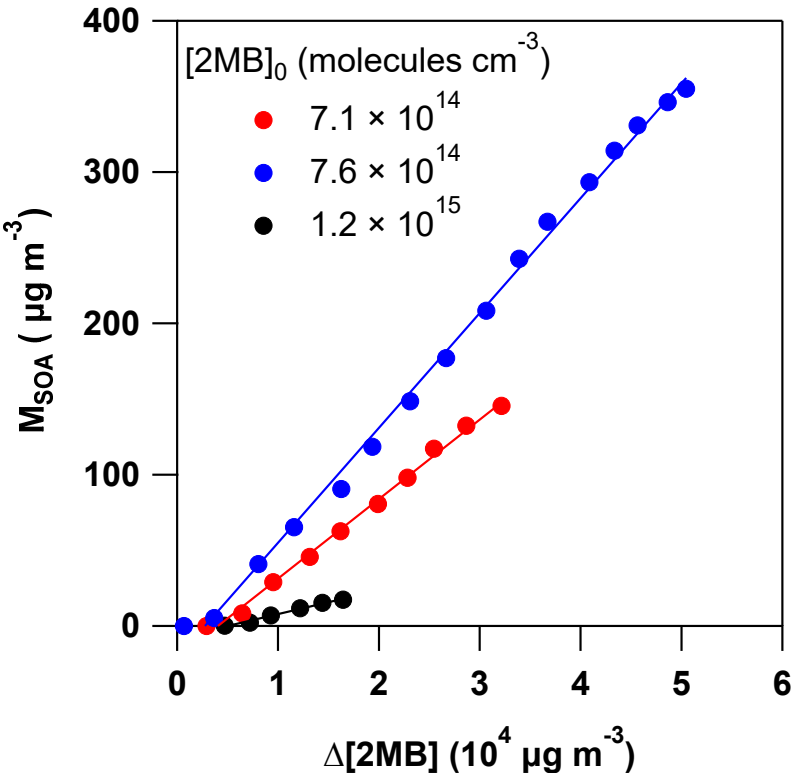

Figure S11: Some examples of the plots of M_{SOA} versus Δ[2MB] used to determine Y_{SOA}.

The size distribution of the particles formed in the Cl + 2MB reaction is shown in terms of the normalized particle number, *d*N/*d*logDp, and mass, *d*M/*d*logDp, in **Fig. S12**. After 2 min of reaction, particles of ca.

90 nm of diameter were formed and started to increase in concentration (particles cm^{-3}) and diameter as reaction elapsed. After 10 min, the particle number $dN/d\log Dp$ for a diameter of ca. 150 nm reached a maximum, while the maximum mass $dM/d\log Dp$ was reached at longer times (t = 27 min) and for particles of ca. 500 nm, what caused that the FMPS could not detect the total mass formed at times longer than 13 min in this case. Therefore, the data analysis to obtain Y_{SOA} according to Eq. (3) was done only during the first 12-30 min, depending on the conditions. Y_{SOA} determined under different conditions are listed in **Table S3**, ranging between 0.16 % and 0.76 %, and showing a negative dependence on $[2MB]_0/[Cl_2]_0$.

Table S3. Results of Y_{SOA} under different conditions.

$[2MB]_0$ (10^{14} molecules cm^{-3})	$[Cl_2]_0$ (10^{14} molecules cm^{-3})	$[2MB]_0/[Cl_2]_0$	Y_{SOA} (%)
6.9	10.3	0.67	0.62 ± 0.04
5.6	6.5	0.85	0.58 ± 0.02
7.6	8.9	0.86	0.76 ± 0.02
7.1	7.5	0.96	0.53 ± 0.02
7.4	5.4	1.4	0.66 ± 0.02
12	8.7	1.4	0.52 ± 0.05
7.2	4.8	1.5	0.30 ± 0.01
13	8.2	1.6	0.44 ± 0.03
12	6	2	0.16 ± 0.02

Y_{SOA} was observed to increase as the maximum value of M_{SOA} detected in the experiment increased. In previous works (Antiñolo et al., 2019; Antiñolo et al., 2020), this trend was described by the gas/particle absorption model proposed by Pankow (Pankow, 1994a, b) and fitted to the equation proposed by Odum et al. (1996). However, in this work it was not possible to know the maximum M_{SOA} formed in the experiment due to instrumental limitations as depicted in **Fig. S12b**, and thus our data were not fitted with the gas/particle absorption model.

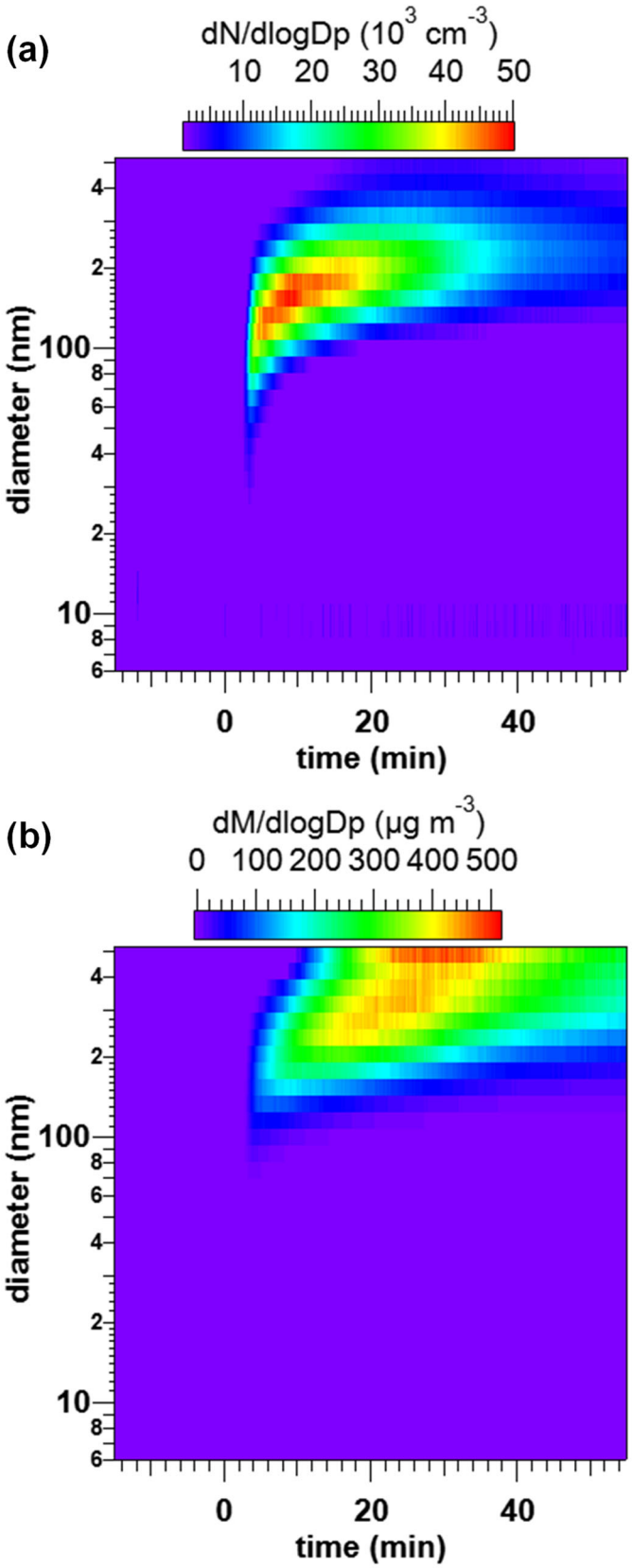

Figure S12: Evolution of the size of the SOA generated in the 2MB + Cl reaction in terms of the normalized particle number (a) and mass (b). Reaction starts at t= 0 min and ends at t= 40 min.

5. Mechanism: UV Photolysis of 2MB and the Cl+2MB reaction

Table S4 lists the corrected product yields for butanone, acetaldehyde, and methylglyoxal obtained in the Cl-reaction of 2MB by different detection methods. This table also shows the formation yields for butanone and butane from the broadband photolysis of 2MB using FTIR as a detection method.

Table S4. Summary of the product yields obtained in this work.

Cl reaction		
Compound	**Detection method**	**Yield (%)**
Butanone	FTIR	53.1 ± 1.6
	PTR-ToF-MS	34.9 ± 0.6
Acetaldehyde	FTIR	-
	PTR-ToF-MS	67.9 ± 0.8
Methylglyoxal	FTIR	-
	PTR-ToF-MS	14.8 ± 0.2
Photolysis reaction		
Compound	**Detection method**	**Yield (%)**
Butane	FTIR	9.80 ± 0.31
Butanone	FTIR	14.8 ± 0.5

In Figs. S13, and S14, the proposed mechanisms that interpret the observed stable products in the photolysis of 2MB and its reaction with Cl atoms are schematized.

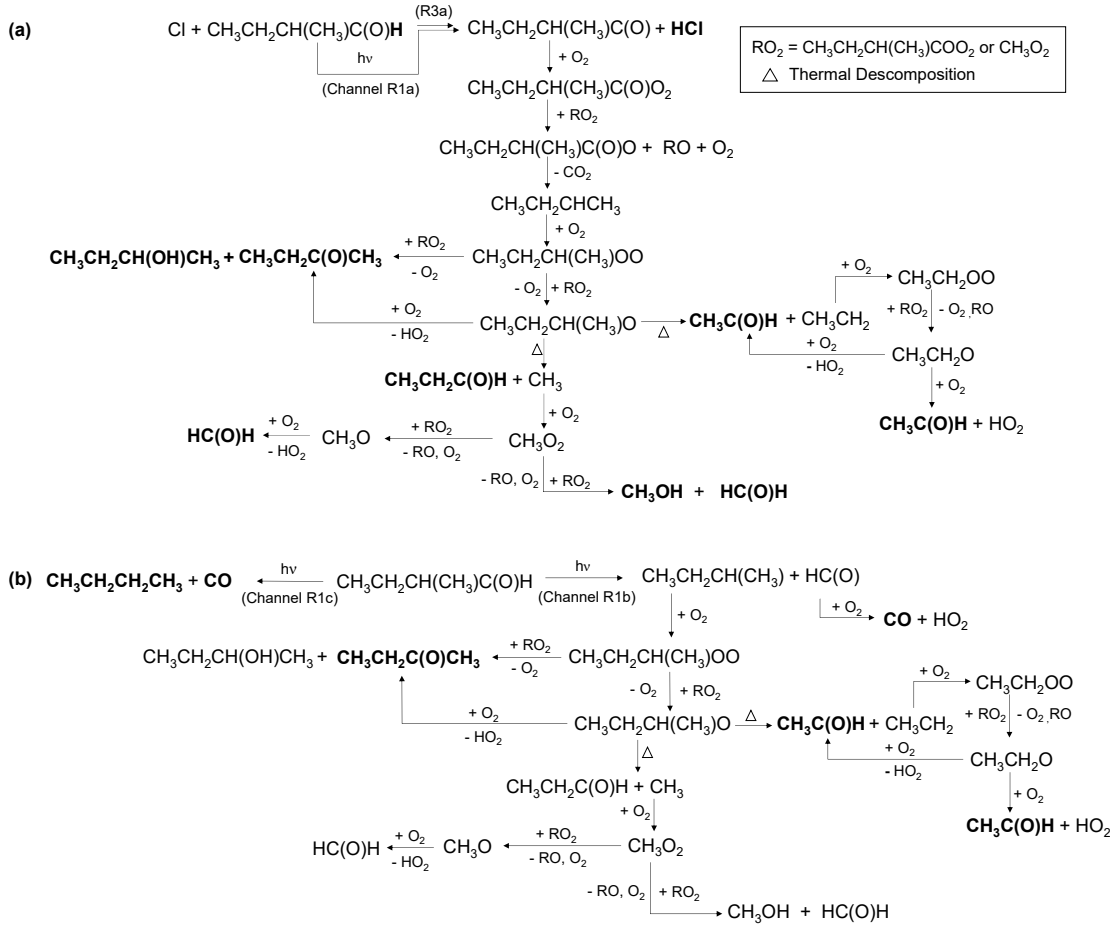

Figure S13: Proposed mechanism for the reaction of 2-methylbutanal considering a) photolysis and aldehydic H-abstraction channel by Cl, b) photodissociation via α -cleavage of the carbon-carbon bond (channel R1b) and molecular elimination of CO (channel R1c). Formation of hydroperoxides (ROOH) is not included for ease of presentation given that they were not detected and that they can be degraded by Cl reaction yielding the same products.

Figure S14: Proposed mechanism for the H-abstraction reaction of 2-methylbutanal with Cl: a) from -CH- group, b) from -CH_2- group, and c) and d) from methyl groups. Note that H-abstraction from the formyl group is depicted in **Figure S11a**. Formation of hydroperoxides (ROOH) is not included for ease of presentation given that they were not detected and that they can be degraded by Cl reaction yielding the same products.

References

Albaladejo, J., Ballesteros, B., Jiménez, E., Martín, P., and Martínez, E.: A PLP–LIF kinetic study of the atmospheric reactivity of a series of C4–C7 saturated and unsaturated aliphatic aldehydes with OH, Atmospheric Environment, 36, 3231-3239, https://doi.org/10.1016/S1352-2310(02)00323-0, 2002.

Antiñolo, M., Jiménez, E., and Albaladejo, J.: Temperature effects on the removal of potential HFC replacements, $CF_3CH_2CH_2OH$ and $CF_3(CH_2)_2CH_2OH$, initiated by OH radicals, Environ. Sci. Technol., 45, 4323-4330, https://doi.org/10.1021/es103931s, 2011.

Antiñolo, M., Asensio, M., Albaladejo, J., and Jiménez, E.: Gas-Phase Reaction of trans-2-Methyl-2-butenal with Cl: Kinetics, Gaseous Products, and SOA Formation, Atmosphere, 11, 715, https://doi.org/10.3390/atmos11070715, 2020.

Antiñolo, M., Olmo, R. d., Bravo, I., Albaladejo, J., and Jiménez, E.: Tropospheric fate of allyl cyanide (CH_2=$CHCH_2CN$): Kinetics, reaction products and secondary organic aerosol formation, Atmospheric Environment, 219, 117041, https://doi.org/10.1016/j.atmosenv.2019.117041, 2019.

Blázquez, S., Antiñolo, M., Nielsen, O. J., Albaladejo, J., and Jiménez, E.: Reaction kinetics of $(CF_3)_2CFCN$ with OH radicals as a function of temperature (278–358K): a good replacement for greenhouse SF_6?, Chemical Physics Letters, 687, 297-302, https://doi.org/10.1016/j.cplett.2017.09.039, 2017.

Ceacero-Vega, A. A., Ballesteros, B., Bejan, I., Barnes, I., Jiménez, E., and Albaladejo, J.: Kinetics and Mechanisms of the Tropospheric Reactions of Menthol, Borneol, Fenchol, Camphor, and Fenchone with Hydroxyl Radicals (OH) and Chlorine Atoms (Cl), The Journal of Physical Chemistry A, 116, 4097-4107, https://doi.org/10.1021/jp212076g, 2012.

Hallquist, M., Wenger, J. C., Baltensperger, U., Rudich, Y., Simpson, D., Claeys, M., Dommen, J., Donahue, N. M., George, C., Goldstein, A. H., Hamilton, J. F., Herrmann, H., Hoffmann, T., Iinuma, Y., Jang, M., Jenkin, M. E., Jimenez, J. L., Kiendler-Scharr, A., Maenhaut, W., McFiggans, G., Mentel, T. F., Monod, A., Prévôt, A. S. H., Seinfeld, J. H., Surratt, J. D., Szmigielski, R., and Wildt, J.: The formation, properties and impact of secondary organic aerosol: current and emerging issues, Atmospheric Chemistry and Physics, 9, 5155-5236, https://doi.org/10.5194/acp-9-5155-2009, 2009.

Jiménez, E., Lanza, B., Garzón, A., Ballesteros, B., and Albaladejo, J.: Atmospheric degradation of 2-butanol, 2-methyl-2-butanol, and 2,3-dimethyl-2-butanol: OH kinetics and UV absorption cross sections, J. Phys. Chem. A, 109, 10903-10909, https://doi.org/10.1021/jp054094g, 2005.

Linstrom, P. J. and Mallard, W. G.: NIST Chemistry WebBook, NIST Standard Reference Database Number 69, National Institute of Standards and Technology, Gaithersburg MD, 20899 [dataset], https://doi.org/10.18434/T4D303, 2018.

Martínez, E., Albaladejo, J., Jiménez, E., Notario, A., and Aranda, A.: Kinetics of the reaction of CH_3S with NO_2 as a function of temperature, Chemical Physics Letters, 308, 37-44, https://doi.org/10.1016/S0009-2614(99)00579-5, 1999.

Odum, J. R., Hoffmann, T., Bowman, F., Collins, D., Flagan, R. C., and Seinfeld, J. H.: Gas/Particle Partitioning and Secondary Organic Aerosol Yields, Environmental Science & Technology, 30, 2580-2585, https://doi.org/10.1021/es950943+, 1996.

Pankow, J. F.: An absorption model of gas/particle partitioning of organic compounds in the atmosphere, Atmospheric Environment, 28, 185-188, https://doi.org/10.1016/1352-2310(94)90093-0, 1994a.

Pankow, J. F.: An absorption model of the gas/aerosol partitioning involved in the formation of secondary organic aerosol, Atmospheric Environment, 28, 189-193, https://doi.org/10.1016/1352-2310(94)90094-9, 1994b.

Ródenas, M.: IR spectrum: 2-Oxopropanal || Methylglyoxal || Pyruvaldehyde, AERIS [dataset], https://doi.org/10.25326/DY39-2H37, 2017.

Sanders, S. P., Abbatt, J., Barker, J. R., Burkholder, J. B., Driedl, R. R., Golden, D. M., Huie, R. E., Kolb, C. E., Kurylo, M. J., Moortgat, G. K., Orkin, V. L., and Wine, P. H.: Chemical Kinetics and Photochemical Data for Use in Atmospheric Studies, Evaluation No. 17, JPL Publication 10-6, Jet Propulsion Laboratory, Pasadena, http://jpldataeval.jpl.nasa.gov, 2011.